Applied Catalysis B: Environmental 219 (2017) 123–131

Contents lists available at ScienceDirect

Applied Catalysis B: Environmental

journal homepage: www.elsevier.com/locate/apcatb

AgIn dendrite catalysts for electrochemical reduction of CO_2 to CO

Hyanjoo Park[a,1], Jihui Choi[a,1], Hoyoung Kim[a], Eunkyoung Hwang[a], Don-Hyung Ha[a], Sang Hyun Ahn[b,*], Soo-Kil Kim[a,*]

[a] School of Integrative Engineering, Chung-Ang University, 84 Heukseokno, Dongjak-gu, Seoul, 06974, Republic of Korea
[b] School of Chemical Engineering and Material Science, Chung-Ang University, 84 Heukseokno, Dongjak-gu, Seoul, 06974, Republic of Korea

ARTICLE INFO

Article history:
Received 14 June 2017
Received in revised form 24 June 2017
Accepted 14 July 2017
Available online 17 July 2017

Keywords:
AgIn dendrite
Electrocatalyst
Electrodeposition
Electrochemical carbon dioxide reduction

ABSTRACT

In this work, the catalytic activities of electrodeposited Ag and AgIn bimetallic dendrites have been explored for electrochemical reduction of CO_2 to CO. In the case of Ag dendrites, the Ag crystal structure was found to be affected by the deposition potential and showed different Ag(220)/Ag(111) ratios. The Faradaic efficiencies to produce CO increased as this ratio increased, whereas the partial current densities for CO generation were found to have a stronger relationship with the roughness of the Ag catalyst. The electrodeposition of AgIn was carried out to investigate the effect of addition of In and its content on the catalytic performance, while maintaining the dendritic morphology. The crystal structures of AgIn dendrites were found to vary with the amount of added In, demonstrating a linear increase in the ratio Ag(220)/Ag(111) with increasing In content and a positive impact on the production of CO. Furthermore, there was a competition between the suppression of the hydrogen evolution reaction (HER) vs. the decrement in the amount of active Ag with increasing addition of In. It was found that these complementary effects resulted in a superior CO Faradaic efficiency of AgIn dendrites with a volcano shaped curve based on the In content. The complementary effect on the catalytic activity could be extended to the various reduction potentials, indicating the significant effect of HER suppression at highly negative reduction potentials.

© 2017 Elsevier B.V. All rights reserved.

1. Introduction

An attractive method for solving the issue of global warming resulting from increased greenhouse gas emissions involves the electrochemical reduction of carbon dioxide (CO_2) [1–4] into valuable fuels such as carbon monoxide (CO) [5–8], formate ($HCOO^-$) [9–14], methane (CH_4) [15–17] and methanol (CH_3OH) [15,18,19]. This process can be made carbon-free when the electrochemical system is operated using electricity obtained from renewable energy sources [20]. However, as CO_2 is thermodynamically and chemically stable, it is less reactive. This suggests that a large overpotential is required to reduce it electrochemically [21]. Furthermore, in the operating potential range for CO_2 reduction, the protons in the aqueous electrolyte are competitively reduced to hydrogen, which results in problems of decreased efficiency of energy input and purity of the gaseous products. Therefore, it is essential to develop a highly active and selective catalyst that enhances the reduction of CO_2 and simultaneously suppresses the hydrogen evolution reaction (HER) [22,23] for the production of high purity C1 fuels.

While Au is known to be the best catalyst for the electrochemical reaction producing CO [24–26], its practical use is limited by its high cost. Alternatively, Ag has been recognized as one of the more attractive candidates owing to its reasonable activity and moderate cost compared to Au [6,27,28]. Thus, the challenges in the development of Ag catalysts for practical applications include further enhancement of activity and reduction of the cost. Based on the benchmarking of different strategies that have been suggested for the development of electrocatalysts required for various energy conversion devices during the last few decades, it has been found that morphological and compositional control is the most effective way to achieve this objective [1,2,29–32]. In addition to the modification of intrinsic activity, the enlarged electrochemical surface area (ECSA) plays an important role in its practical applications [8,29,30]. The state-of-the-art catalysts demonstrate a high performance with a particular highly populated facet in controlled morphology [35,36] and a properly modified electronic structure in controlled composition [31,32,37,38].

* Corresponding authors.
E-mail addresses: shahn@cau.ac.kr (S.H. Ahn), sookilkim@cau.ac.kr (S.-K. Kim).
[1] These authors contributed equally.

http://dx.doi.org/10.1016/j.apcatb.2017.07.038
0926-3373/© 2017 Elsevier B.V. All rights reserved.

Based on these strategies, many studies have been conducted for the development of Ag-based electrocatalysts [30,39–41]. In recent reports of the morphological control of metallic Ag [1,2,29,30], the CO Faradaic efficiency of nanoporous Ag at −0.60 V_{RHE} [42,43], Ag nano-corals at −0.48 V_{RHE} [44], and Ag foam at −0.99 V_{RHE} [45] was over 90%. This efficiency is much higher than that of Ag nanoparticles and Ag foil. Ge et al. have also reported the bubble-templated electrodeposited Ag foam which exhibits a CO Faradaic efficiency of ∼92% at −0.86 V_{RHE} [46]. A high performance of mesostructured Ag inverse opal [47] and thin-layer porous Ag [48] has recently been reported for the generation of CO from CO_2. The origin of higher efficiency of the catalyst can be explained by a high population of certain facets in the controlled structure [43]. However, fabrication and utilization of the metallic Ag nanostructures has sometimes been limited by the large amounts of Ag required (e.g. ∼40 mg cm^{-2}) [42], resulting in a severe cost problem.

Another strategy to improve the intrinsic catalytic activity involves fabrication of intermetallic Ag-based catalysts [6,7,22,27,28,30,38]. However, this approach is relatively rare compared to morphological control. For experimental purposes, Cu is an effective choice to prepare bimetallic catalysts with Ag for CO production [7]. Although the pure Ag dendritic catalyst showed higher CO Faradaic efficiency compared to the bimetallic Ag-Cu dendritic catalysts, the $Ag_{57}Cu_{43}$ catalyst demonstrated a higher Ag mass activity at −0.86 V_{RHE} than the pure Ag catalyst. A similar enhancement of catalyst performance for the CO production is also observed with Ag-Zn bimetallic [49] and alloy [50] catalysts. In this strategy, metals such as Cu, Zn, and In, which are used together with Ag, are known to have poor activity for the hydrogen evolution reaction (HER) [1,16,22,51,52]. Pérez-Ramírez et al. have reported the effect of a support on a Ag catalyst for the reduction of CO_2 to produce CO [53]. With an $In(OH)_3$ support, the Ag catalyst showed a CO Faradaic efficiency of ∼68% at −0.6 V_{RHE} which was higher than that achieved with either a C support (∼30%) or In_2O_3 support (∼40%) [53].

In this study, electrodeposited Ag and AgIn bimetallic dendrites have been reported, which were designed by taking advantages of both morphological and compositional control for the electrochemical reduction of carbon dioxide. Notably, In is known as one of the less active metals for HER owing to its high overpotential for the reaction [54–56]. In addition, the electrodeposition method provides a simple means toward easy control of the morphology and composition. The highly negative deposition potential facilitates the fabrication of a dendritic structure with a large surface roughness. The varying metal precursor ratio in the deposition bath enables an easy control of the composition of AgIn bimetallic catalysts while maintaining their dendritic structure. After careful investigations on material properties, the catalytic performances of the prepared Ag and AgIn bimetallic dendrites were explored. At a certain morphology and composition of AgIn bimetallic dendrite, a higher CO Faradaic efficiency and partial current density compared with pure Ag dendrite was observed, owing to the complementary effect originating from the controlled crystal morphology and composition.

2. Experimental

2.1. Preparation of Ag and AgIn dendrites

For the pretreatment of the substrate, a commercial Cu foil (Sigma Aldrich, thickness: 0.0255 mm, 349208, 99.98%) was immersed in a solution of 0.02 M $C_6H_8O_7$ (citric acid, Sigma Aldrich, 99%, C0759) and 0.034 M KOH (DAEJUNG, 93%, 6597-4400) to eliminate the native oxide formed at the surface [57–59]. A thin Ag layer was fabricated by the displacement of Ag on the Cu foil for 20 s using a mixture of 0.059 M $AgNO_3$ (Sigma Aldrich, 99.9%, 209139), 0.58 M $(NH_4)_2SO_4$ (Sigma Aldrich, 99.0%, A5132), and 3.78 M NH_4OH (Wako, 30%, 016-03146) solutions as the electrolyte. With the fabrication of the thin Ag layer, the adhesive property was increased for the following Ag electrodeposition process [60] and the unwanted exposure of Cu to the CO_2 reduction electrolyte could be prevented. For the electrodeposition of Ag, a conventional three-electrode cell system was prepared by using a lab-made Teflon cell. The Ag/Cu foil was used as a working electrode while the Pt wires were used as both counter and reference electrodes. The electrolyte for Ag electrodeposition was composed of 0.01 M Ag_2SO_4 (DAEJUNG, 99.5%, 7524-4125), 1.0 M H_2SO_4 (JUNSEI, 95%, 83010-0350), and 0.05 M $C_6H_8O_7$, whereas the electrolyte for AgIn electrodeposition was a mixture of x M Ag_2SO_4 (where x = 0.003, 0.005, 0.007, and 0.010), 0.01 M $In_2(SO_4)_3$ (Sigma Aldrich, 98%, 57151), 1.0 M H_2SO_4, and 0.05 M $C_6H_8O_7$. The details of the electrodeposition process for preparing Ag and AgIn dendrites are summarized in Table S1. The deposition potential and time were controlled by using potentiostat (Autolab PGSTAT 302 N, Metrohm).

2.2. Characterization techniques

The morphology of all the samples including commercial foils was imaged by using a field emission scanning electron microscope (FE-SEM, SIGMA, Carl Zeiss). X-ray diffraction (XRD, New D8-Advance, BRUKER-AXS) analysis was performed for all samples to identify their crystal structure at a scan rate of 5° min^{-1}. X-ray photoelectron spectroscopy (XPS, ThermoFisher Scientific, K-alpha+) measurement was performed on Ag and AgIn dendrites in order to investigate their surface composition.

2.3. Electrochemical reduction of CO_2

The electrochemical reduction of carbon dioxide was carried out in a lab-made polycarbonate H-type cell. The cathode and anode parts of the cell were separated by Nafion® NRE-212 proton exchange membrane. The cell capacity for both cathode and anode sections was 120 mL and these were filled by 100 mL of 0.5 M $KHCO_3$ (DAEJUNG, 99.5%, 6580-4400) electrolyte. The electrochemical reaction was carried out using a three-electrode system. The Ag and AgIn dendrites were used as the working electrode with an area of 4.9 cm^2 exposed to the electrolyte. The Pt gauze and saturated calomel electrode (SCE) were used as the counter and reference electrodes, respectively. CO_2 was injected into the catholyte at a rate of 300 mL min^{-1} for at least 45 min before the start of the experiment to saturate the solution. Then, the chronoamperometric measurements were performed at various potential values of −1.1 ∼ −1.7 V_{SCE} for 30 min. The catalytic activity of commercial Ag foil (Alfa Aesar, 43081, 99.9%, thickness: 0.05 mm) was also tested under the same conditions.

The concentrations of the generated CO and H_2 from the cathode part were measured by gas chromatography (GC, 7890A, Agilent 7890A). The inlet of the GC equipment was connected to the top of the cathode section. During the chronoamperometric measurements, CO_2 gas was continuously injected at a constant rate of 10 sccm using a mass flow controller (MFC, MKS Instruments Inc.), in order to saturate the CO_2 reactant in the catholyte and to carry the product gas into the GC. The product gas was analyzed by both thermal conductivity detector (TCD) and flame ionization detector (FID). The current efficiency named as Faradaic efficiency (FE) was calculated by comparing the amounts of detected CO and H_2 with the amount of electrochemically applied charge during the corresponding reduction time.

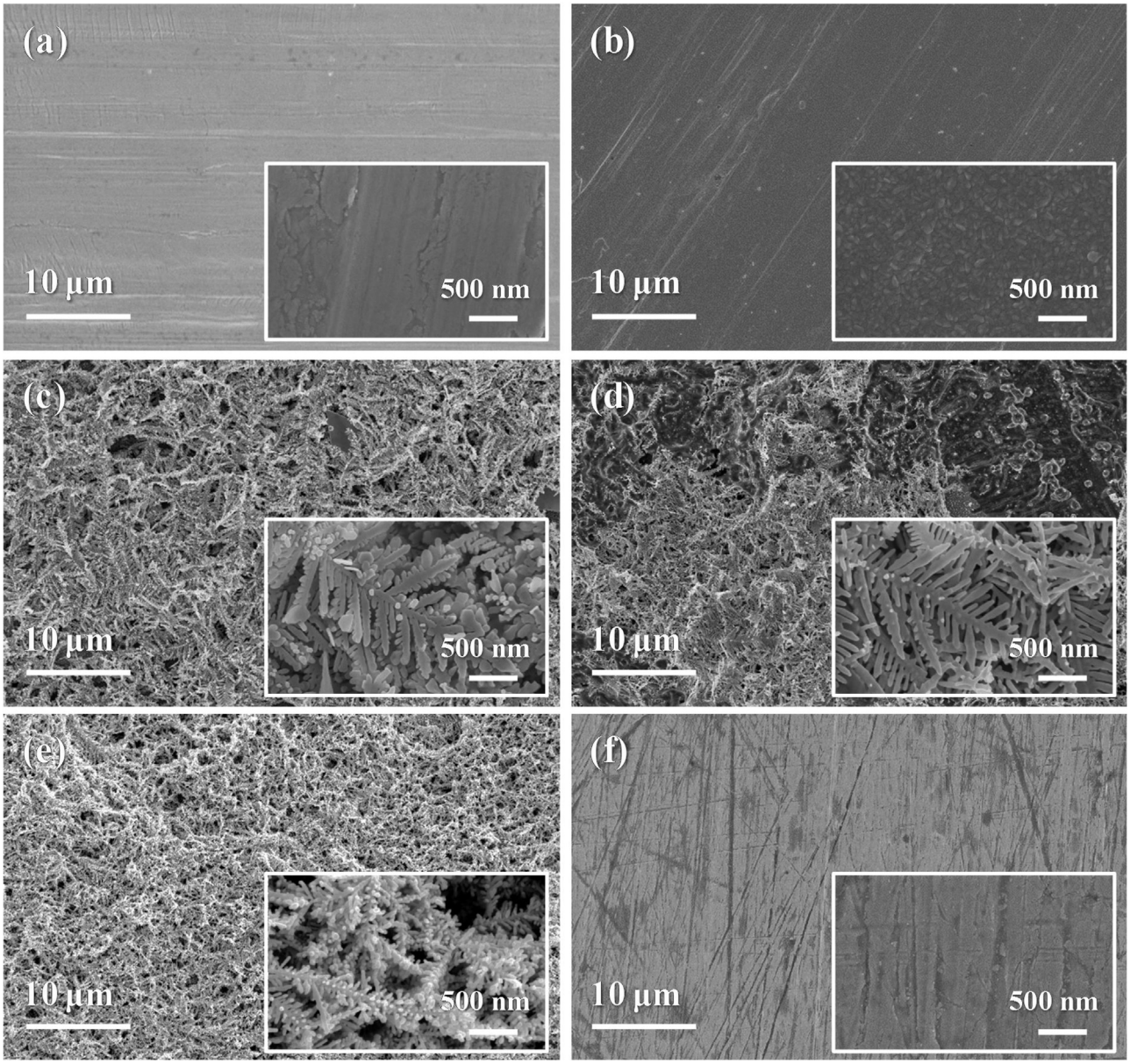

Fig. 1. FE-SEM images of (a) commercial Cu foil, (b) Ag displaced Cu foil (Ag/Cu foil), electrodeposited Ag dendrites on Ag/Cu foil at the deposition potential of (c) −0.8 V_{NHE}, (d) −1.3 V_{NHE}, (e) −1.5 V_{NHE}, and (f) commercial Ag foil.

3. Results and discussion

3.1. Characterization of Ag catalysts

Fig. 1a displays the FE-SEM images of the commercial Cu foil that has a smooth surface on the imaged scale. After displacement of Ag for 20 s, aggregated polygonal clusters appeared at the surface of the foil, as shown in the inset of Fig. 1b. Fig. 1c–e demonstrate the morphology of the Ag dendrites electrodeposited on the Ag/Cu foil. At the deposition potential of −0.8 V_{NHE} (NHE: normal hydrogen electrode), the leaf-shaped Ag dendrites could be observed (Fig. 1c) and their branches were slightly grown at a more negative deposition potential of −1.3 V_{NHE} (Fig. 1d). At the deposition potential of −1.5 V_{NHE}, a much-roughened Ag surface with a high population of relatively short branches could be observed (Fig. 1e). It can be reasoned that these dendritic structures were obtained only on applying a highly negative deposition potential owing to the mass-transfer limitation of Ag ions in the electrolyte [61]. Furthermore, the extreme generation of hydrogen bubbles under high overpotential conditions during electrodeposition also affects the morphology of the Ag dendrites [62]. As a reference to the electrodeposited Ag dendrites, a commercial Ag foil was also imaged (Fig. 1f).

The crystal structures of the deposited and commercial samples were determined by XRD analysis, as shown in Fig. 2a. For commercial Cu foil, sharp metallic Cu(111), (200), and (220) peaks were observed at 43.3°, 50.4°, and 74.1°, respectively [JCPDS#04-0836]. The peaks were slightly decreased after Ag displacement with the presence of a weak Ag(111) peak at 38.1°. After the formation of Ag dendrites by electrodeposition, the intensity of the Ag(111) peak was considerably increased. The metallic Ag peaks of the Ag dendrites appeared at 44.3°, 64.4°, and 77.5° for Ag(200), Ag(220), and Ag(311), respectively [JCPDS#04-0783]. As summarized in Fig. 2b, the intensity of these Ag facets varied depending on the deposition potential employed for Ag dendrite formation. However, the Ag(220)/Ag(111) intensity ratio decreased by the negative

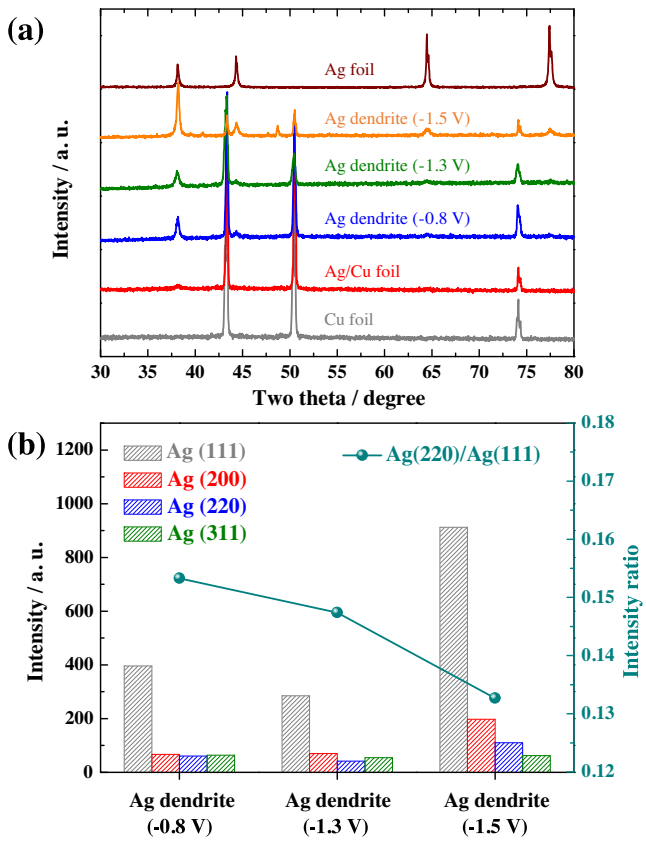

Fig. 2. (a) XRD patterns of the commercial foils and electrodeposited Ag dendrites. (b) Ag peak intensity and Ag(220)/Ag(111) intensity ratio of electrodeposited Ag dendrites.

shift of deposition potential. This trend is somewhat different with that described previously [28], presumably because of the different electrolyte compositions that were utilized in addition to the different types of Ag precursor. For comparison, the peak intensities and Ag(220)/Ag(111) ratios for smoother Ag foils are shown in Fig. S1.

3.2. Electrochemical reduction of CO_2 on Ag catalysts

Fig. 3a shows the results of the chronoamperometric analysis of Ag/Cu foil, Ag dendrites, and commercial Ag foil for the reduction of CO_2 in a CO_2-purged 0.5 M $KHCO_3$ electrolyte at $-1.5\,V_{SCE}$ for the duration of 1800s. The recorded current densities were in following order: Ag dendrite (−1.5 V) > Ag dendrite (−1.3 V) > Ag dendrite (−0.8 V) > Ag/Cu foil ≥ commercial Ag foil, which conceivably represent the effect of different active surface areas (Fig. 1) for the reduction reactions of both CO_2 and proton. The catalytic performance represented by the Faradaic efficiency for CO and H_2 production is summarized in Fig. 3b. Owing to their significantly smoother surfaces and much lower active areas, the Ag/Cu and commercial Ag foils showed the relatively low CO Faradaic efficiencies of 37.2% and 30.2% at $-1.5\,V_{SCE}$, respectively. The measured current, with the exception of CO and H_2 production, might also be used for other reactions such as CH_4 and CH_3OH production [63]. The latter reactions have not been analyzed in this study. In case of the Ag dendrites deposited on Ag/Cu foil, the CO Faradaic efficiencies were drastically improved, which was consistent with the findings previously reported in literature that discuss a significant effect of Ag roughness on the CO Faradaic efficiency [42,44,46,47]. The Ag dendrites electrodeposited at $-0.8\,V_{NHE}$ demonstrated the highest CO Faradaic efficiency of 65.6%. As the Ag deposition potential became more negative, the CO Faradaic efficiency of Ag dendrites was found to gradually decrease. On comparing these results for the different Ag dendrites, it appears that this decay of CO Faradaic efficiency is closely related to the XRD peak intensity ratio of Ag(220)/Ag(111), as shown in Fig. 3c. This trend is in good agreement with previously reported literature [28,43,59]. However, a much lower CO Faradaic efficiency was obtained with the significantly smoother Ag catalysts of Ag/Cu and commercial Ag foil, even though they had higher intensity ratios of Ag(220)/Ag(111) compared to electrodeposited Ag dendrites. This observation suggests that the surface roughness (Fig. 1) and surface area overwhelm the effects of crystallographic structures in this particular case. On comparison of the amounts of CO produced, which are expressed in terms of CO partial currents (Fig. 3d), it was found that the Ag dendrites still exhibited much larger CO partial currents than those of the foils. However, the order of CO partial currents among the different dendrites (Ag dendrite (−1.5 V) > Ag dendrite (−1.3 V) > Ag dendrite (−0.8 V)) were opposite to that of CO Faradaic efficiency, as shown in Fig. 3b. Thus, it is clear that the numerous branches of Ag dendrites electrodeposited at $-1.5\,V_{NHE}$ had the largest surface area among the Ag dendrites, which led to the highest current density.

3.3. Characterization of AgIn catalysts

In order to further improve the intrinsic activity of the Ag dendrite, co-electrodeposition of AgIn was conducted on a Ag/Cu foil substrate. For the formation of the AgIn dendritic structure, a highly negative deposition potential of $-1.5\,V_{NHE}$ was applied for 180 s with varying ratios of the In^{3+}/Ag^{+} precursor concentrations (as 1.0, 1.4, 2.0, and 3.3) in the deposition bath, as shown in Fig. 4. The morphologies of all AgIn dendrites observed at low and high magnification were barely different from that of Ag dendrite at the same deposition potential and time (see Fig. 1e). The AgIn dendrites have a leaf-shaped structure with negligible difference in branch length on a scale of several hundred nanometers. Thus, it could be said that the morphology of AgIn dendrites was not a strong function of the ratio of Ag^{+}/In^{3+} precursor concentrations in the deposition bath.

The XPS analysis was conducted on the Ag and AgIn dendrites in order to investigate their surface composition (Fig. S2). The peak areas of the Ag 3d and In 3d spectra with due consideration of the sensitivity factors gave the compositional information for all AgIn dendrites. With the increasing ratio of In^{3+}/Ag^{+} precursor concentration from 1.0 to 3.3, the atomic surface concentration of AgIn dendrites was increased from 8.9 to 40.5%, as demonstrated in Fig. S3a. The nomenclature of Ag and AgIn dendrites was determined by the surface composition of Ag and In. The XRD patterns of Ag and AgIn dendrites are given in Fig. 5a. In all samples, the metallic Ag peaks appeared at 38.1°, 44.3°, 64.4°, and 77.5° [JCPDS # 04-0783] with decreased intensities upon inclusion of In. No peaks corresponding to either the Ag-In alloys or metallic In were observed, which is a different aspect of the crystalline intermetallic compound ($AgIn_2$) that is formed by sequentially depositing In and Ag from a sulfamate bath at room temperature [64]. It is also noteworthy that the peak intensities at 43.3° and 50.4° corresponding to Cu increased with the addition of In. It is difficult to precisely interpret the enhanced peaks of underlying Cu. The exposure of the underlying Cu substrate becomes possible when the deposited In reacts with displacement-deposited Ag layer to form the Ag-In compound [64], which may be either amorphous or nanocrystalline in this case. Involvement of In oxides such as In_2O_3 (440) [65] may contribute to the peak at 50.4° as well.

The peak intensities for Ag(111), (200), (220), and (311) were calculated from the XRD patterns, as shown in Fig. S4. The overall intensities corresponding to Ag gradually decreased with increas-

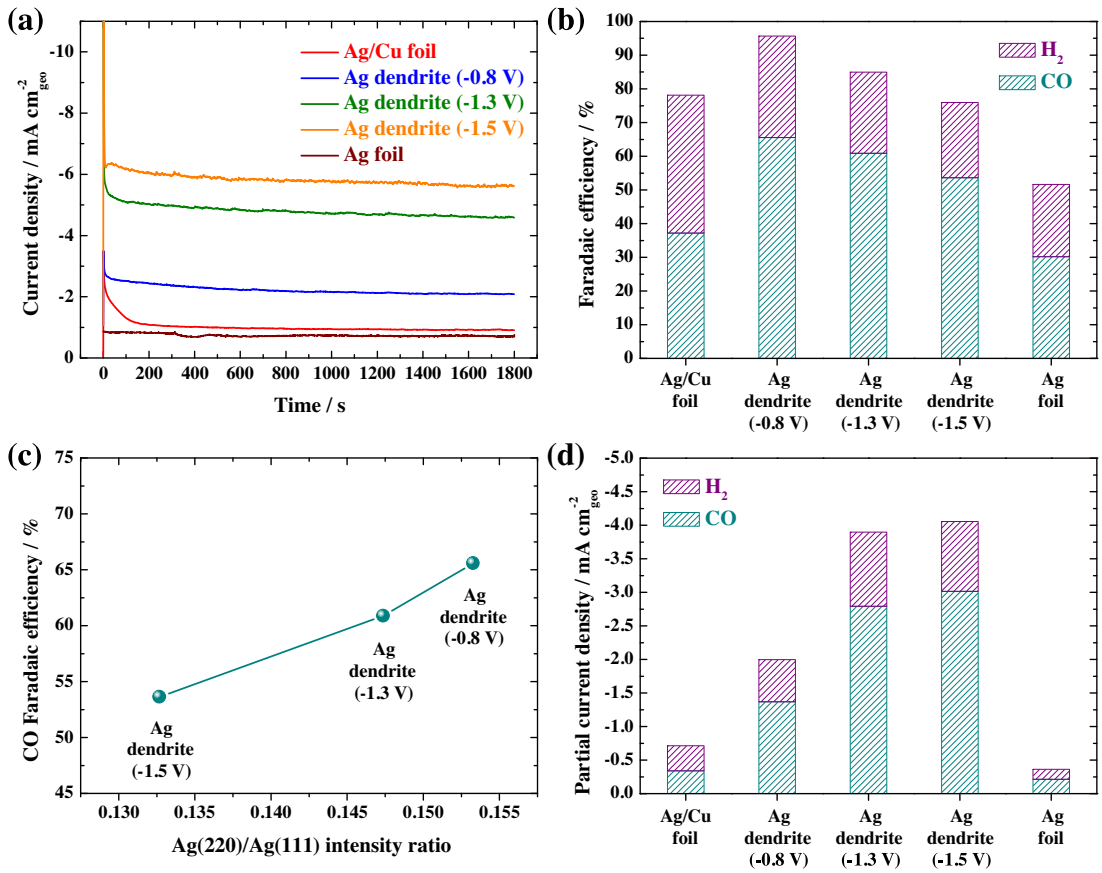

Fig. 3. (a) Chronoamperometries in a CO_2-purged 0.5 M $KHCO_3$ electrolyte at −1.5 V_{SCE} for 1800 s. (b) Faradaic efficiency for CO and H_2 production. (c) CO Faradaic efficiency as a function of Ag(220)/Ag(111) intensity ratio. (d) Partial current density for CO and H_2 production.

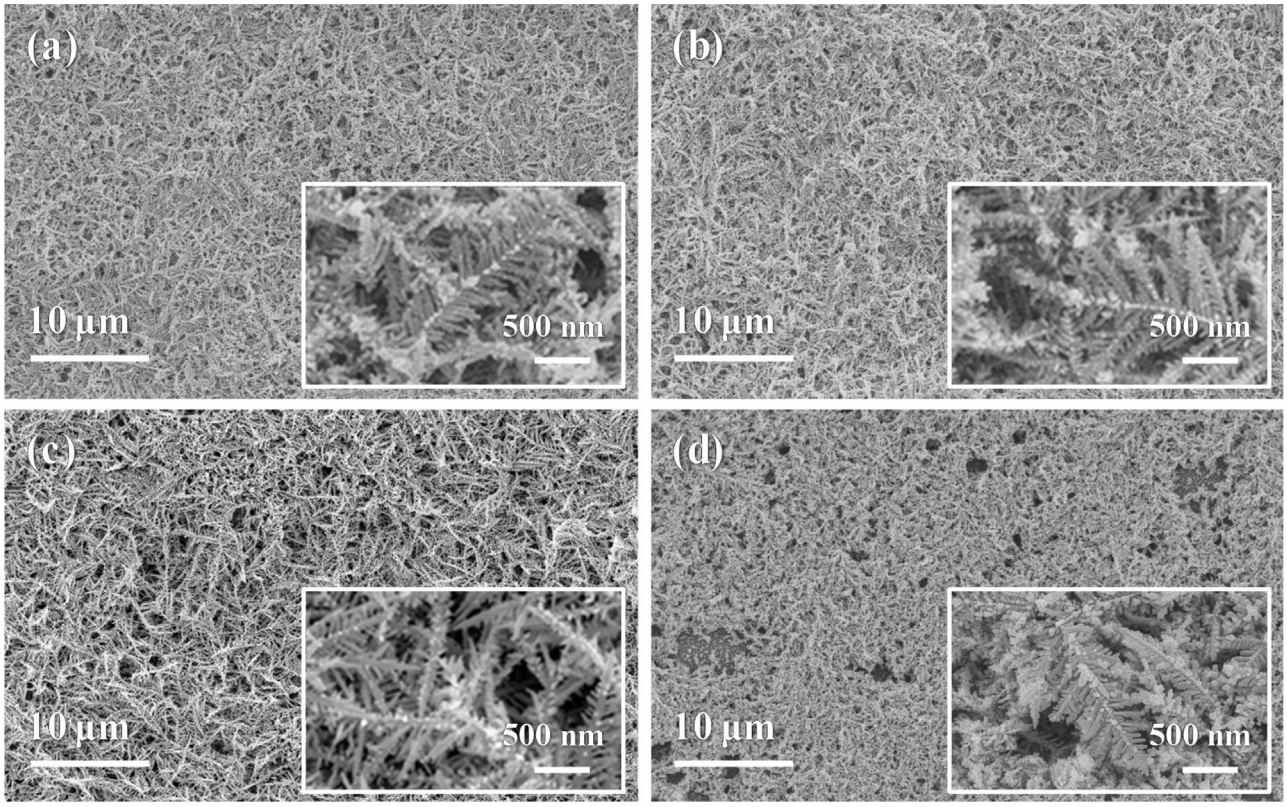

Fig. 4. FE-SEM images of AgIn dendrites electrodeposited at deposition potential of −1.5 V_{NHE} for 180 s in the electrolyte containing the In^{3+}/Ag^{+} precursor ratio of (a) 1.0, (b) 1.4, (c) 2.0, and (d) 3.3.

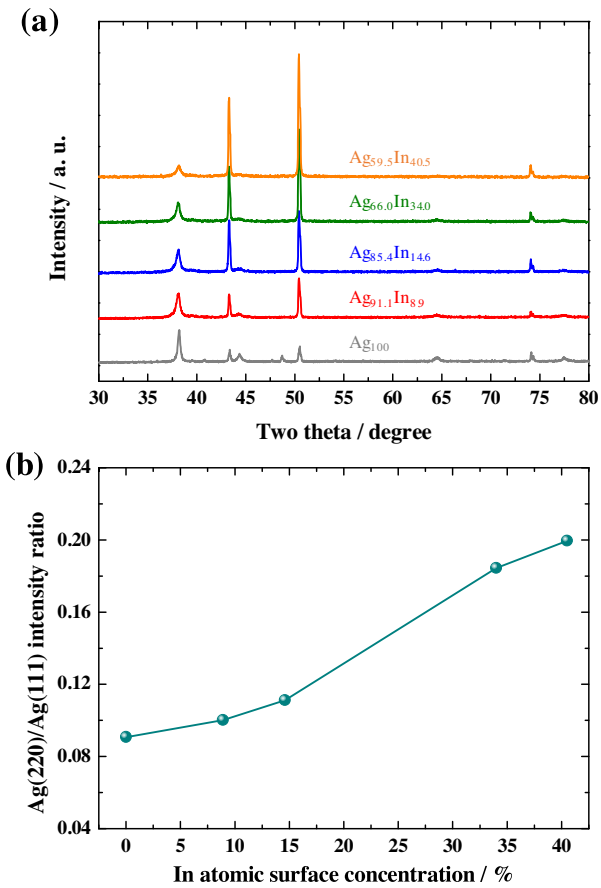

Fig. 5. (a) XRD patterns of electrodeposited Ag_{100} and AgIn dendrites. (b) Ag(220)/Ag(111) intensity ratio as a function of In atomic surface concentration.

ing surface concentrations of atomic In because the deposition currents partially contributed to the reduction of the In ions, resulting in the lower amount of Ag formation. However, the Ag(220)/Ag(111) ratio gradually increased from 0.09 to 0.20 for the Ag_{100} and $Ag_{59.5}In_{40.5}$ catalysts, respectively (Fig. 5b).

3.4. Electrochemical reduction of CO_2 on AgIn catalysts

Fig. 6a shows the CAs of Ag_{100} and AgIn catalysts in CO_2-purged 0.5 M $KHCO_3$ electrolyte at −1.3 V_{SCE} in the duration of 1800s. All AgIn dendrites demonstrated lower current densities than the Ag_{100} catalyst. Fig. 6b shows the CO Faradaic efficiency as a function of In atomic surface concentration. With a lower In concentration of 8.9%, the CO Faradaic efficiency was recorded as 56.5%, which was slightly higher than that obtained by using the Ag_{100} catalyst (51.5%). Notably, with further increase in the concentration of In, an obvious enhancement of the CO Faradaic efficiency was observed. The maximum CO Faradaic efficiency of 68.8% was obtained with the $Ag_{66.0}In_{34.0}$ catalyst and this value subsequently decreased to 65.3% when the In content was 40.5%. This is in generally good accordance with the trend of the Ag(220)/Ag(111) intensity ratio shown in Fig. 5b, except some points such as the bending observed at high In content. In order to establish accordance between the intensity ratio and CO Faradaic efficiency, it is necessary to consider that the absolute amounts of the corresponding facets decrease with the In content (Fig. 5a), in spite of the increasing trend of the (220)/(111) ratio. Therefore, besides the contribution of the intensity ratio, competitive effects between the suppression of HER and the deterioration of CO production by increasing amount of In (and thus decreasing amount of the active Ag) play important roles. It is reasonable to conclude that a strong complementary effect existed for the CO Faradaic efficiency between the two parameters. At low and mid-levels of In, the addition of In resulted in an effective suppression of the HER reaction. For example, at all CO_2 reduction potentials, the $Ag_{66.0}In_{34.0}$ catalyst demonstrated a higher CO Faradaic efficiency than the Ag_{100} catalyst, accompanied with a significant suppression of HER [1,16,22], as shown in Fig. 6c and S5. It is also noteworthy that a substantial enhancement of the CO partial current density was observed especially at −1.7 V_{SCE} (where a severe HER took place), indicating a strong inhibition of HER as a result of addition of In and its practical advantages in the production of CO (Fig. 6d). Therefore, the overall decrease in the reduction currents for AgIn in Fig. 6a occurred primarily owing to the suppression of HER by the added In. However, with higher In content, the quantitative decrease in the Ag content of the catalysts had a negative impact on the production of CO, resulting in a volcano-like shape of the CO Faradaic efficiency curve studied in relation to the In content (shown in Fig. 5b).

Fig. 7a shows the CO Faradaic efficiencies of the developed catalysts, as calculated from Fig. S6 and GC data, and their dependence on the CO_2 reduction potential and the catalyst composition. At a lower potential of −1.1 V_{SCE}, where HER was not severe, the positive effect of In addition was not obvious. However, the CO Faradaic efficiency in the potential range of −1.3 ∼ −1.7 V_{SCE} was significantly improved with all of the AgIn catalysts. The maximum CO Faradaic efficiency was recorded as 75.5% with $Ag_{85.4}In_{14.6}$ catalyst at −1.5 V_{SCE} and this catalyst showed 39.6% enhanced CO Faradaic efficiency at −1.7 V_{SCE} compared with the Ag_{100} catalyst. Meanwhile, the advantageous HER suppression upon addition of In was observed in H_2 Faradaic efficiency, regardless of reduction potential and catalyst composition (Fig. 7b). In the case of CO partial current density (Fig. 7c), the $Ag_{66.0}In_{34.0}$ catalyst exhibited higher values compared with Ag_{100} catalyst at all potentials. It should be emphasized that at a very negative reduction potential of −1.7 V_{SCE} with severe HER, the much higher CO partial current density was observed with all AgIn catalysts, which was also supported by the H_2 partial current density, as shown in Fig. 7d. All AgIn catalysts demonstrated the HER suppression effect at all potentials. In addition, the mass activities of Ag and AgIn catalysts were calculated by dividing the CO partial current density by the loading catalyst mass (Fig. S3b), as illustrated in Fig. S7. At a lower potential range, the mass activities of Ag_{100} and $Ag_{59.5}In_{40.5}$ catalysts had similar values. However, the $Ag_{59.5}In_{40.5}$ catalyst demonstrated much higher values in more negative potential ranges, indicating the positive effect of addition of In. Furthermore, the catalyst developed in this study exhibited higher mass activity in comparison with the nanoporous (NP) Ag catalyst previously reported by literature [42]. Therefore, the AgIn catalysts developed in this work show an enhanced activity in the reduction of CO_2 to CO via the modification of geometric/crystallographic structures as well as the suppression of the competitive HER.

4. Conclusion

The electrodeposited Ag and AgIn dendrites used as catalysts for electrochemical reduction of CO_2 demonstrated a significant relationship between CO production and their morphologies and compositions. In case of electrodeposited Ag dendrites, the CO Faradaic efficiency was strongly affected by the Ag(220)/Ag(111) ratio, while the CO partial current density showed a dependence on the roughness of the catalyst. After adding In to the Ag dendrites under optimized conditions, the CO Faradaic efficiency of the AgIn catalysts exhibited a volcano-like behavior based on the In content owing to the competition between the HER suppression and decreasing amounts of active Ag with increasing In content.

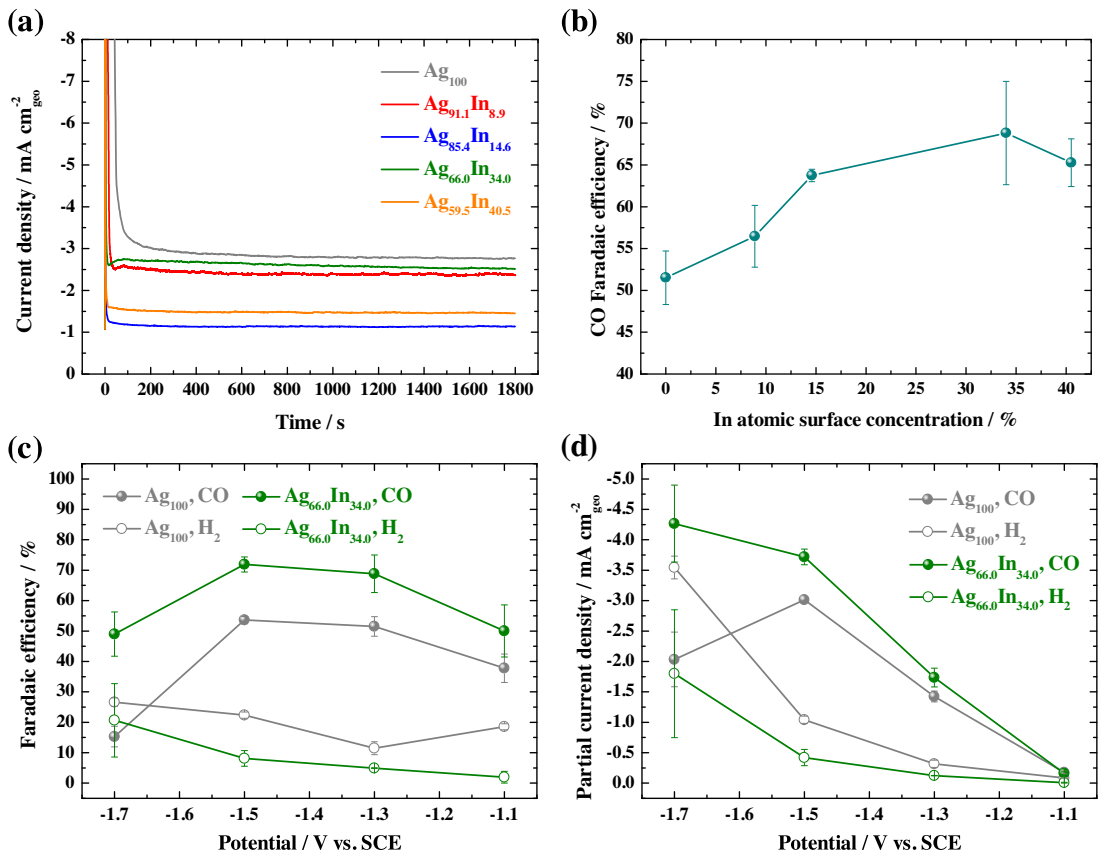

Fig. 6. (a) Chronoamperometries of Ag_{100} and AgIn dendrite catalysts in a CO_2-purged 0.5 M $KHCO_3$ electrolyte at −1.3 V_{SCE} for 1800 s. (b) CO Faradaic efficiency depending on the In atomic surface concentration. (c) Faradaic efficiency and (d) partial current density of Ag_{100} and $Ag_{66.0}In_{34.0}$ dendrite catalyst as a function of potential.

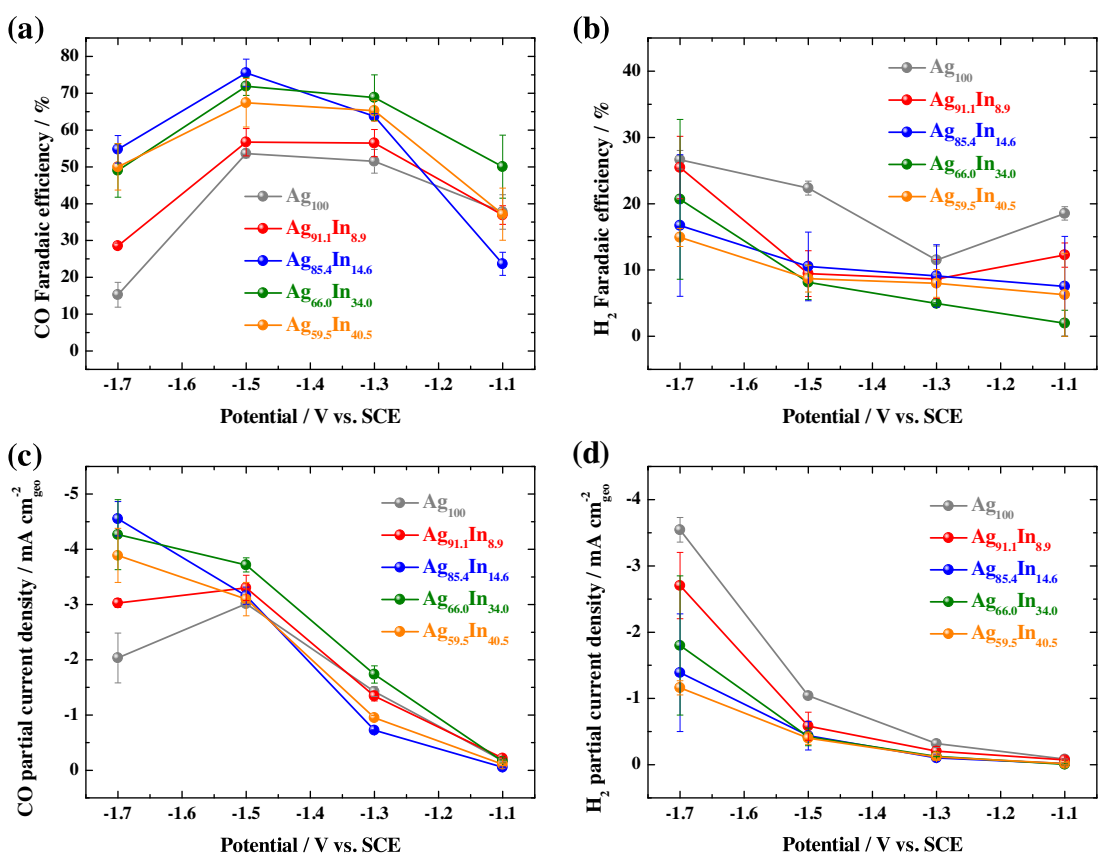

Fig. 7. (a) CO and (b) H_2 Faradaic efficiency, (c) CO and (d) H_2 partial current density of Ag_{100} and AgIn dendrite catalysts as a function of reduction potential.

The enhanced Ag(220)/Ag(111) intensity ratio of AgIn catalysts also contributed to the CO Faradaic efficiency. When various In compositions and reduction potentials were studied, the complementary effect was still found to exist. In conclusion, the catalytic performance of Ag dendrites was enhanced by adding In, which led to much higher selectivity in the electrochemical reduction of CO_2 to CO rather than HER in highly negative potential region.

Acknowledgements

This work was supported by the National Research Foundation of Korea (NRF) Grant funded by the Korean Government MSIP (2016M1A2A2937146 and 2015R1C1A1A01055708), MOE (2016R1D1A1B03931963), and Korea CCS R&D Center (KCRC) (2014M1A8A1049349).

Appendix A. Supplementary data

Supplementary data associated with this article can be found, in the online version, at http://dx.doi.org/10.1016/j.apcatb.2017.07.038.

References

[1] Q. Lu, F. Jiao, Electrochemical CO_2 reduction: electrocatalyst, reaction mechanism, and process engineering, Nano Energy 29 (2016) 439–456.
[2] Z.-L. Wang, C. Li, Y. Yamauchi, Nanostructured nonprecious metal catalysts for electrochemical reduction of carbon dioxide, Nano Today 11 (2016) 373–391.
[3] R. Kortlever, J. Shen, K.J. Schouten, F. Calle-Vallejo, M.T. Koper, Catalysts and reaction pathways for the electrochemical reduction of carbon dioxide, J. Phys. Chem. Lett. 6 (2015) 4073–4082.
[4] R.J. Lim, M. Xie, M.A. Sk, J.-M. Lee, A. Fisher, X. Wang, K.H. Lim, A review on the electrochemical reduction of CO_2 in fuel cells, metal electrodes and molecular catalysts, Catal. Today 233 (2014) 169–180.
[5] M.S. Jee, H.S. Jeon, C. Kim, H. Lee, J.H. Koh, J. Cho, B.K. Min, Y.J. Hwang, Enhancement in carbon dioxide activity and stability on nanostructured silver electrode and the role of oxygen, Appl. Catal. B: Environ. 180 (2016) 372–378.
[6] K. Sun, L. Wu, W. Qin, J. Zhou, Y. Hu, Z. Jiang, B. Shen, Z. Wang, Enhanced electrochemical reduction of CO_2 to CO on Ag electrocatalysts with increased unoccupied density of states, J. Mater. Chem. A 4 (2016) 12616–12623.
[7] J. Choi, M.J. Kim, S.H. Ahn, I. Choi, J.H. Jang, Y.S. Ham, J.J. Kim, S.-K. Kim, Electrochemical CO_2 reduction to CO on dendritic Ag–Cu electrocatalysts prepared by electrodeposition, Chem. Eng. J. 299 (2016) 37–44.
[8] Q. Li, J. Fu, W. Zhu, Z. Chen, B. Shen, L. Wu, Z. Xi, T. Wang, G. Lu, J.J. Zhu, S. Sun, Tuning Sn-catalysis for electrochemical reduction of CO_2 to CO via the core/shell Cu/SnO_2 structure, J. Am. Chem. Soc. 139 (2017) 4290–4293.
[9] X. Zhang, T. Lei, Y. Liu, J. Qiao, Enhancing CO_2 electrolysis to formate on facilely synthesized Bi catalysts at low overpotential, Appl. Catal. B: Environ. 218 (2017) 46–50.
[10] S.Y. Choi, S.K. Jeong, H.J. Kim, I.-H. Baek, K.T. Park, Electrochemical reduction of carbon dioxide to formate on tin–lead alloys, ACS Sustain. Chem. Eng. 4 (2016) 1311–1318.
[11] O. Scialdone, A. Galia, G.L. Nero, F. Proietto, S. Sabatino, B. Schiavo, Electrochemical reduction of carbon dioxide to formic acid at a tin cathode in divided and undivided cells: effect of carbon dioxide pressure and other operating parameters, Electrochim. Acta 199 (2016) 332–341.
[12] C. Zhao, J. Wang, Electrochemical reduction of CO_2 to formate in aqueous solution using electro-deposited Sn catalysts, Chem. Eng. J. 293 (2016) 161–170.
[13] Z. Bitar, A. Fecant, E. Trela-Baudot, S. Chardon-Noblat, D. Pasquier, Electrocatalytic reduction of carbon dioxide on indium coated gas diffusion electrodes-comparison with indium foil, Appl. Catal. B: Environ. 189 (2016) 172–180.
[14] B. Innocent, D. Pasquier, F. Ropital, F. Hahn, J.-M. Léger, K.B. Kokoh, FTIR spectroscopy study of the reduction of carbon dioxide on lead electrode in aqueous medium, Appl. Catal. B: Environ. 94 (2010) 219–224.
[15] P. Hirunsit, W. Soodsawang, J. Limtrakul, CO_2 electrochemical reduction to methane and methanol on copper-based alloys: theoretical insight, J. Phys. Chem. C 119 (2015) 8238–8249.
[16] J. Shen, R. Kortlever, R. Kas, Y.Y. Birdja, O. Diaz-Morales, Y. Kwon, I. Ledezma-Yanez, K.J. Schouten, G. Mul, M.T. Koper, Electrocatalytic reduction of carbon dioxide to carbon monoxide and methane at an immobilized cobalt protoporphyrin, Nat. Commun. 6 (2015) 8177.
[17] T.A. Maark, B.R.K. Nanda, CO and CO_2 electrochemical reduction to methane on Cu Ni, and Cu_3Ni (211) surfaces, J. Phys. Chem. C 120 (2016) 8781–8789.
[18] P.K. Giesbrecht, D.E. Herbert, Electrochemical reduction of carbon dioxide to methanol in the presence of benzannulated dihydropyridine additives, ACS Energy Lett. 2 (2017) 549–555.
[19] M. Irfan Malik, Z.O. Malaibari, M. Atieh, B. Abussaud, Electrochemical reduction of CO_2 to methanol over MWCNTs impregnated with Cu_2O, Chem. Eng. Sci. 152 (2016) 468–477.
[20] Y. Song, R. Peng, D.K. Hensley, P.V. Bonnesen, L. Liang, Z. Wu, H.M. Meyer, M. Chi, C. Ma, B.G. Sumpter, A.J. Rondinone, High-selectivity electrochemical conversion of CO_2 to ethanol using a copper nanoparticle/N-doped graphene electrode, ChemistrySelect 1 (2016) 6055–6061.
[21] H.K. Lim, H. Shin, W.A. Goddard 3rd, Y.J. hwang, B.K. Min, H. Kim, Embedding covalency into metal catalysts for efficient electrochemical conversion of CO_2, J. Am. Chem. Soc 136 (2014) 11355–11361.
[22] C. Kim, T. Eom, M.S. Jee, H. Jung, H. Kim, B.K. Min, Y.J. Hwang, Insight into electrochemical CO_2 reduction on surface-molecule-mediated Ag nanoparticles, ACS Catal. 7 (2017) 779–785.
[23] E.E. Benson, C.P. Kubiak, A.J. Sathrum, J.M. Smieja, Electrocatalytic and homogeneous approaches to conversion of CO2 to liquid fuels, Chem. Soc. Rev. 38 (2009) 89–99.
[24] Y. Fang, J.C. Flake, Electrochemical reduction of CO_2 at functionalized Au electrodes, J. Am. Chem. Soc. 139 (2017) 3399–3405.
[25] E. Andrews, S. Katla, C. Kumar, M. Patterson, P. Sprunger, J. Flake, Electrocatalytic reduction of CO_2 at Au nanoparticle electrodes: effects of interfacial chemistry on reduction behavior, J. Electrochem. Soc. 162 (2015) F1373–F1378.
[26] E.R. Cave, J.H. Montoya, K.P. Kuhl, D.N. Abram, T. Hatsukade, C. Shi, C. Hahn, J.K. Norskov, T.F. Jaramillo, Electrochemical CO_2 reduction on Au surfaces: mechanistic aspects regarding the formation of major and minor products, Phys. Chem. Chem. Phys. 19 (2017) 15856–15863.
[27] M. Ma, B.J. Trzesniewski, J. Xie, W.A. Smith, Selective and efficient reduction of carbon dioxide to carbon monoxide on oxide-derived nanostructured silver electrocatalysts, Angew. Chem. Int. Ed. 55 (2016) 9748–9752.
[28] Y.S. Ham, S. Choe, M.J. Kim, T. Lim, S.-K. Kim, J.J. Kim, Electrodeposited Ag catalysts for the electrochemical reduction of CO_2 to CO, Appl. Catal. B: Environ. 208 (2017) 35–43.
[29] M. Liu, Y. Pang, B. Zhang, P. De Luna, O. Voznyy, J. Xu, X. Zheng, C.T. Dinh, F. Fan, C. Cao, F.P. de Arquer, T.S. Safaei, A. Mepham, A. Klinkova, E. Kumacheva, T. Filleter, D. Sinton, S.O. Kelley, E.H. Sargent, Enhanced electrocatalytic CO_2 reduction via field-induced reagent concentration, Nature 537 (2016) 382–386.
[30] S. Liu, H. Tao, L. Zeng, Q. Liu, Z. Xu, Q. Liu, J.L. Luo, Shape-dependent electrocatalytic reduction of CO_2 to CO on triangular silver nanoplates, J. Am. Chem. Soc. 139 (2017) 2160–2163.
[31] X. Zhao, B. Luo, R. Long, C. Wang, Y. Xiong, Composition-dependent activity of Cu–Pt alloy nanocubes for electrocatalytic CO_2 reduction, J. Mater. Chem. A 3 (2015) 4134–4138.
[32] D. Kim, J. Resasco, Y. Yu, A.M. Asiri, P. Yang, Synergistic geometric and electronic effects for electrochemical reduction of carbon dioxide using gold-copper bimetallic nanoparticles, Nat. Commun. 5 (2014) 4948–4955.
[35] Q. Lu, J. Rosen, F. Jiao, Nanostructured metallic electrocatalysts for carbon dioxide reduction, ChemCatChem 7 (2015) 38–47.
[36] Y. Li, Q. Liu, W. Shen, Morphology-dependent nanocatalysis: metal particles, Dalton Trans. 40 (2011) 5811–5826.
[37] S.Y. Choi, S.K. Jeong, K.T. Park, Electrocatalytic reduction of carbon dioxide on Sn-Pb alloy electrodes, J. Clim. Change Res. 7 (2016) 231–236.
[38] Z. Chang, S. Huo, W. Zhang, J. Fang, H. Wang, The tunable and highly selective reduction products on Ag@Cu bimetallic catalysts toward CO_2 electrochemical reduction reaction, J. Phys. Chem. C 121 (2017) 11368–11379.
[39] W. Luc, C. Collins, S. Wang, H. Xin, K. He, Y. Kang, F. Jiao, Ag-Sn bimetallic catalyst with a core-shell structure for CO_2 reduction, J. Am. Chem. Soc. 139 (2017) 1885–1893.
[40] S. Back, M.S. Yeom, Y. Jung, Active sites of Au and Ag nanoparticle catalysts for CO_2 electroreduction to CO, ACS Catal. 5 (2015) 5089–5096.
[41] L.Q. Zhou, C. Ling, M. Jones, H. Jia, Selective CO2 reduction on a polycrystalline Ag electrode enhanced by anodization treatment, Chem. Commun. 51 (2015) 17704–17707.
[42] Q. Lu, J. Rosen, Y. Zhou, G.S. Hutchings, Y.C. Kimmel, J.G. Chen, F. Jiao, A selective and efficient electrocatalyst for carbon dioxide reduction, Nat. Commun. 5 (2014) 3242–3246.
[43] J. Rosen, G.S. Hutchings, Q. Lu, S. Rivera, Y. Zhou, D.G. Vlachos, F. Jiao, Mechanistic insights into the electrochemical reduction of CO_2 to CO on nanostructured Ag surfaces, ACS Catal. 5 (2015) 4293–4299.
[44] Y.-C. Hsieh, S.D. Senanayake, Y. Zhang, W. Xu, D.E. Polyansky, Effect of chloride anions on the synthesis and enhanced catalytic activity of silver nanocoral electrodes for CO_2 electroreduction, ACS Catal. 5 (2015) 5349–5356.
[45] R. Daiyan, X. Lu, Y.H. Ng, R. Amal, Highly selective conversion of CO_2 to CO achieved by a three-dimensional porous silver electrocatalyst, ChemistrySelect 2 (2017) 879–884.
[46] H. Wang, Z. Han, L. Zhang, C. Cui, X. Zhu, X. Liu, J. Han, Q. Ge, Enhanced CO selectivity and stability for electrocatalytic reduction of CO_2 on electrodeposited nanostructured porous Ag electrode, J. CO_2 Util. 15 (2016) 41–49.
[47] Y. Yoon, A.S. Hall, Y. Surendranath, Tuning of silver catalyst mesostructure promotes selective carbon dioxide conversion into fuel, Angew. Chem. 128 (2016) 15508–15512.
[48] L. Zhang, Z. Wang, N. Mehio, X. Jin, S. Dai, Thickness- and particle-size-dependent electrochemical reduction of carbon dioxide on thin-layer porous silver electrodes, ChemSusChem 9 (2016) 428–432.

[49] Q. Yu, X. Meng, L. Shi, H. Liu, J. Ye, Superfine Ag nanoparticle decorated Zn nanoplates for the active and selective electrocatalytic reduction of CO_2 to CO, Chem. Commun. 52 (2016) 14105–14108.
[50] T. Hatsukade, K.P. Kuhl, E.R. Cave, D.N. Abram, J.T. Feaster, A.L. Jongerius, C. Hahn, T.F. Jaramillo, Carbon dioxide electroreduction using a silver-zinc alloy, Energy Technol. 5 (2017) 1–8.
[51] P. Saji, A.K. Ganguli, M.A. Bhat, P.P. Ingole, Probing the crystal structure, composition-dependent absolute energy levels, and electrocatalytic properties of silver indium sulfide nanostructures, ChemPhysChem 17 (2016) 1195–1203.
[52] N. Behrooz, A. Ghaffarinejad, N. Sadeghi, Ag/Cu nano alloy as an electrocatalyst for hydrogen production, J. Electroanal. Chem. 782 (2016) 1–8.
[53] G.O. Larrazábal, A.J. Martín, S. Mitchell, R. Hauert, J. Pérez-Ramírez, Synergistic effects in silver–indium electrocatalysts for carbon dioxide reduction, J. Catal. 343 (2016) 266–277.
[54] S. Omanovic, M. M.-Hukovic, Indium as a cathodic material: catalytic reduction of formaldehyde, J. Appl. Electrochem. 27 (1997) 35–41.
[55] S.R. Narayanan, B. Haines, J. Soler, T.I. Valdez, Electrochemical conversion of carbon dioxide to formate in alkaline polymer electrolyte membrane cells, J. Electrochem. Soc. 158 (2011) A167–A173.
[56] C. Ding, A. Li, S.-M. Lu, H. Zhang, C. Li, In situ electrodeposited indium nanocrystals for efficient CO_2 reduction to CO with low overpotential, ACS Catal. 6 (2016) 6438–6443.
[57] S.H. Hong, S.H. Ahn, J. Choi, J.Y. Kim, H.Y. Kim, H.-J. Kim, J.H. Jang, H. Kim, S.-K. Kim, High-activity electrodeposited NiW catalysts for hydrogen evolution in alkaline water electrolysis, Appl. Surf. Sci. 349 (2015) 629–635.
[58] J.Y. Kim, H. Park, H. Kim, E. Hwang, S.H. Ahn, S.-K. Kim, Electrochemical preparation of Ru/Co Bi-layered catalysts on Ti substrates for the oxygen evolution reaction, Bull. Kor. Chem. Soc. 37 (2016) 1270–1277.
[59] H. Park, H. Kim, E. Hwang, S.H. Ahn, S.-K. Kim, J. Nanosci. Nanotechnol. (2017) (accepted to).
[60] J. Yuan, Y. Lai, J. Duan, Q. Zhao, J. Zhan, Synthesis of a beta-cyclodextrin-modified Ag film by the galvanic displacement on copper foil for SERS detection of PCBs, J. Colloid Interf. Sci. 365 (2012) 122–126.
[61] N. Abbasi, P. Shahbazi, A. Kiani, Electrocatalytic oxidation of ethanol at Pd/Ag nanodendrites prepared via low support electrodeposition and galvanic replacement, J. Mater. Chem. A 1 (2013) 9966–9972.
[62] S. Cherevko, X. Xing, C.-H. Chung, Electrodeposition of three-dimensional porous silver foams, Electrochem. Commun. 12 (2010) 467–470.
[63] K.P. Kuhl, T. Hatsukade, E.R. Cave, D.N. Abram, J. Kibsgaard, T.F. Jaramillo, Electrocatalytic conversion of carbon dioxide to methane and methanol on transition metal surfaces, J. Am. Chem. Soc. 136 (2014) 14107–14113.
[64] J. Pin, J.S. Wang, C.C. Lee, Intermetallic reaction between electroplated indium and silver layers, J. Electron. Mater. 38 (2009) 1860–1865.
[65] L. Qin, P.S. Dutta, S. Sawyer, Photoresponse of indium oxide particulate-based thin films fabricated using milled nanorods grown by the self-catalytic vapor?liquid?solid process, Semicon. Sci. Technol. 27 (2012) 045005.